

Improving the Precision of Near-Infrared Stellar Photometry by Modeling the Image Formation Process within a Lossy Detector¹

Kenneth Mighell

National Optical Astronomy Observatory, 950 N. Cherry Ave., Tucson, AZ 85719

ABSTRACT

Current infrared detector technology can produce imagers with non-uniform intrapixel response functions. Cameras based on such detectors can have large systematic errors in the measurement of the total stellar flux. Although this problem can be mitigated by oversampling the stellar image, many near infrared cameras are undersampled in order to achieve a large field of view. The combination of undersampling stellar images with non-uniform detectors is currently diminishing the science return of some infrared imagers onboard the *Hubble Space Telescope* and the *Spitzer Space Telescope*. Large intrapixel quantum efficiency variations can also cause significant systematic position measurement errors. Although the recorded flux and position of point sources is corrupted by using detectors with non-uniform intrapixel response functions, it is still possible to achieve excellent stellar photometry and astrometry — if the image formation process inside the detector is accurately modeled. A practical demonstration of how the precision and accuracy of near infrared stellar photometry can be significantly improved is provided by a detailed analysis of stellar observations obtained with Spitzer’s Infrared Array Camera (IRAC) instrument.

1. PHOTOMETRY AND ASTROMETRY WITH DISCRETE POINT SPREAD FUNCTIONS

The MATPHOT algorithm for precise and accurate stellar photometry and astrometry with discrete (sampled) Point Spread Functions (PSFs) was described in detail by Mighell [1]. The current C-language [2] implementation of the MATPHOT algorithm works with user-provided discrete PSFs consisting of a numerical table represented by a matrix in the form of a FITS image [3]. Discrete PSFs are shifted within an observational model using a 21-pixel-wide damped sinc function [4] and position partial derivatives are computed using a five-point numerical differentiation formula [5]. Precise and accurate stellar photometry and astrometry are achieved with undersampled charge coupled device (CCD) observations by using supersampled discrete PSFs that are sampled 2, 3, or more times more finely than the observational data. Although these numerical techniques are not mathematically perfect, they are sufficiently accurate for precision stellar photometry and astrometry due to photon noise which is present in all astronomical imaging observations. The current photometric reduction code [6] is based on a robust implementation of the Levenberg-Marquardt method of nonlinear least-squares minimization [7–10]. Detailed analysis of simulated *Next Generation Space Telescope* observations demonstrate that millipixel relative astrometry and millimag photometric precision are achievable with complicated space-based discrete PSFs [1].

¹ This work is based on archival data obtained with the *Spitzer Space Telescope*, which is operated by the Jet Propulsion Laboratory, California Institute of Technology under a contract with NASA. Support for this work was provided by an award issued by JPL/Caltech.

2. OBSERVATIONS AND PHOTOMETRIC REDUCTIONS

Sixteen short (0.4 s) calibration observations of the K0 star PPM 9412 were obtained on 2003 October 8 UT with Channel 1 (3.6 μm) of the Infrared Array Camera (IRAC; [11]) onboard the *Spitzer Space Telescope* (see Table 1).

ID	RA_HMS	DEC_DMS	EXPTIME	DATE_OBS	DS_IDENT
1	17h06m11.6s	+73d40m11s	0.4	2003-10-08T11:55:51.356	ads/sa.spitzer#0006875392
2	17h06m11.1s	+73d40m11s	0.4	2003-10-08T12:08:56.748	ads/sa.spitzer#0006876672
3	17h06m10.8s	+73d40m10s	0.4	2003-10-08T12:22:01.538	ads/sa.spitzer#0006876928
4	17h06m10.6s	+73d40m09s	0.4	2003-10-08T12:35:06.524	ads/sa.spitzer#0006877184
5	17h06m11.3s	+73d40m12s	0.4	2003-10-08T12:48:11.510	ads/sa.spitzer#0006877440
6	17h06m10.9s	+73d40m12s	0.4	2003-10-08T13:01:16.496	ads/sa.spitzer#0006877696
7	17h06m10.5s	+73d40m11s	0.4	2003-10-08T13:14:21.489	ads/sa.spitzer#0006877952
8	17h06m10.2s	+73d40m11s	0.4	2003-10-08T13:27:26.471	ads/sa.spitzer#0006878208
9	17h06m11.0s	+73d40m14s	0.4	2003-10-08T13:40:31.472	ads/sa.spitzer#0006878464
10	17h06m10.7s	+73d40m13s	0.4	2003-10-08T13:53:36.446	ads/sa.spitzer#0006878720
11	17h06m10.5s	+73d40m13s	0.4	2003-10-08T14:06:41.436	ads/sa.spitzer#0006878976
12	17h06m10.0s	+73d40m12s	0.4	2003-10-08T14:19:46.422	ads/sa.spitzer#0006879232
13	17h06m11.0s	+73d40m15s	0.4	2003-10-08T14:32:51.423	ads/sa.spitzer#0006879488
14	17h06m10.5s	+73d40m15s	0.4	2003-10-08T15:06:39.788	ads/sa.spitzer#0006879744
15	17h06m10.3s	+73d40m14s	0.4	2003-10-08T15:19:44.785	ads/sa.spitzer#0006880000
16	17h06m10.0s	+73d40m13s	0.4	2003-10-08T15:32:49.763	ads/sa.spitzer#0006880256

Table 1. IRAC Ch1 Observations of PPM 9412

The IRAC basic calibrated data (BCD) images were retrieved from the Spitzer data archive. These observations were analyzed with the imexamine task of NOAO's Image Reduction and Analysis Facility (IRAF; [12–13]) package and a new experimental version of MATPHOT, called MPDZ, which uses the following relative intrapixel quantum efficiency (QE) variation map [14] for IRAC Channel 1 (Ch1),

$$\text{intrapix} = \begin{pmatrix} 0.813 & 0.875 & 0.875 & 0.875 & 0.813 \\ 0.875 & 1.000 & 1.000 & 1.000 & 0.875 \\ 0.875 & 1.000 & 1.000 & 1.000 & 0.875 \\ 0.875 & 1.000 & 1.000 & 1.000 & 0.875 \\ 0.813 & 0.875 & 0.875 & 0.875 & 0.813 \end{pmatrix},$$

and a theoretical IRAC Ch1 PSF [15] for the central region of IRAC Ch1 (see Fig. 1).

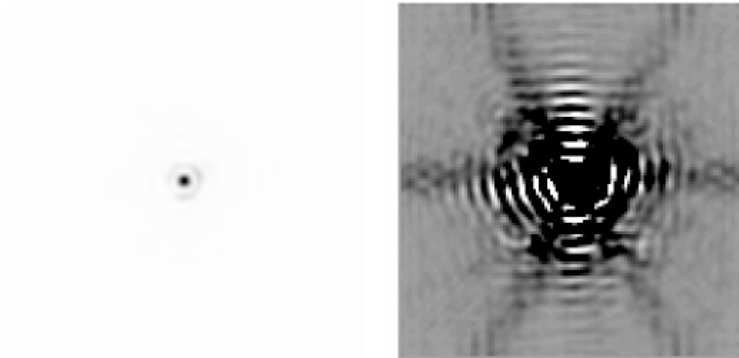


Fig. 1. A theoretical 5x5 supersampled version of the IRAC PSF for the central region of Ch1 [15]. The left side of 4 shows a linear stretch of the PSF and the right side shows a log stretch. Although the PSF appears to be reasonable in the linear stretch, which emphasizes the bright central core, the log stretch shows the numerous weak higher-spatial-frequency features of this very complicated PSF. IRAC Ch1 PSFs are significantly undersampled by the IRAC Ch1 camera [11].

3. SQUARE APERTURE PHOTOMETRY

Square aperture photometry with a 21x21 pixel box centered on the star was done using the interactive “m” keyboard command of IRAF’s imexamine task. Fig. 2 shows a 5.6% peak-to-peak spread in these square aperture flux measurements.

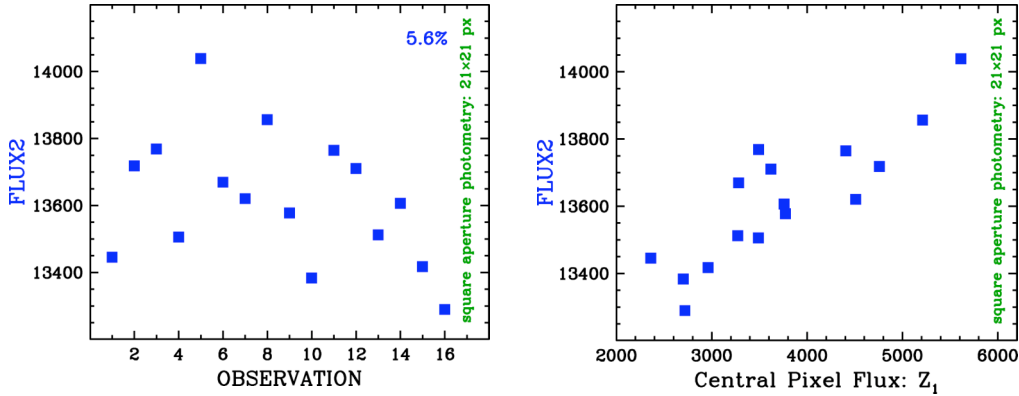


Fig. 2. Square aperture photometry (21x21 pixels)

The variation in flux seen in Fig. 2 is not completely random. The right graph of Fig. 2 shows that the total stellar flux is correlated with the amount of flux found in the central pixel. Examination of the individual observations reveal that the observations with the most stellar flux have stellar images that are centered in the middle of a pixel while those observations with the least stellar flux are centered on a pixel corner. This same effect is seen in Fig. 3 which is taken from the IRAC Data Handbook [16].

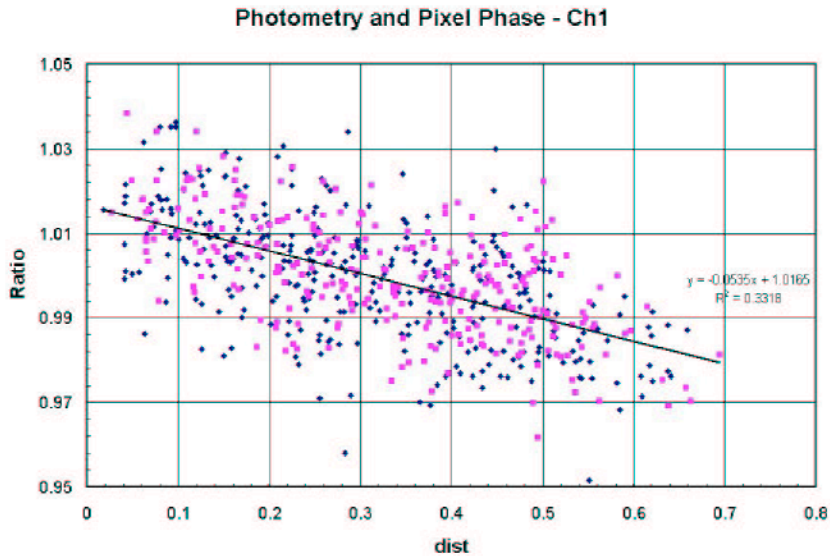


Fig. 3. Normalized measured flux density (y-axis) is plotted against the distance of the source centroid from the center of a pixel (source: Fig. 5.1 of the IRAC Data Handbook [16]).

The flux density of a point source measured from IRAC images depends on the exact location where the peak of the stellar image (the Point Response Function) falls within the central pixel of the stellar image. This effect is due to the variations in the quantum efficiency of a pixel, and combined with the undersampling of the PRF, it is most severe in Channel 1 [16]. The correction can be as much as 4% peak to peak.

4. CIRCULAR APERTURE PHOTOMETRY

Circular aperture photometry centered on the star with a radius of 10 pixels was done using the interactive “a” keyboard command of IRAF’s imexamine task. Fig. 4 shows a 5.3% peak-to-peak spread in the raw circular aperture flux measurements (open circles). Applying the recommended Ch1 flux correction (solid line in Fig. 3) from the IRAC Data Handbook reduces the peak-to-peak spread to 4.9% (filled circles).

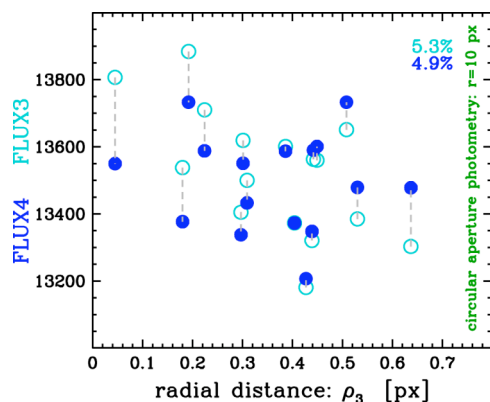


Fig. 4. Circular aperture photometry (radius of 10 pixels)

Hoping to improve the measurement by reducing the contribution of background noise, circular aperture photometry centered on the star with a radius of 5 pixels was done using the interactive “a” keyboard command of IRAF’s imexamine task. Fig. 5 shows a 4.5% peak-to-peak spread in the raw circular aperture flux measurements (open circles). Applying the recommended Ch1 flux correction (solid line in Fig. 3) from the IRAC Data Handbook reduces the peak-to-peak spread to 3.5% (filled circles).

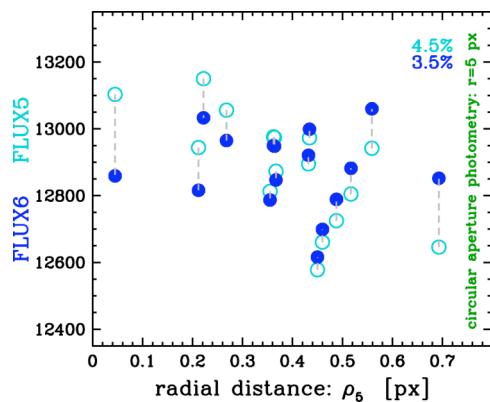


Fig. 5. Circular aperture photometry (radius of 10 pixels)

5. MATPHOT SIMULATIONS

Ten thousand IRAC Ch1 observations of a single star on a flat background were simulated and analyzed with MPDZ. Each stellar observation was simulated using the theoretical 5x5 supersampled IRAC Ch1 PSF shown in Fig. 1; a star with 10^6 electrons was located near the center of an field of 60x60 pixels on a flat background of 100 electrons. The horizontal axis of the left graph of Fig. 6 shows the subpixel offset (distance) the center of a star is from the middle of a pixel; stars centered near the middle of a pixel will have small offset values while stars located near the corner of a pixel will have offsets near 0.7 px. The vertical axis of the left graph of Fig. 6 shows the absolute flux ratio of the total fluxes divided by the true flux of 10^6 electrons. The cyan points show the *observed* absolute flux ratios and the blue points show the measured absolute flux ratios as reported by MPDZ. Note that

while the *average* stellar observation suffered an absolute flux loss of about 9%, stars centered near the middle of a pixel suffered, on average, an absolute flux loss of about 7% as compared to an absolute flux loss of about 11% for stars centered near a pixel corner. It is important to note that *the vertical scatter seen in the observed flux ratios is not random but systematic*; a simple radial correction function can only partially recover the lost flux. The *measured* absolute flux ratios are clustered around unity and are not a function of subpixel offset; the vertical scatter seen in the measured absolute flux ratios is random. By modeling the image formation process within the detector, MPDZ was able to fully recover all of the stellar flux lost due to the non-uniform IRAC Ch1 intrapixel quantum efficiency variations.

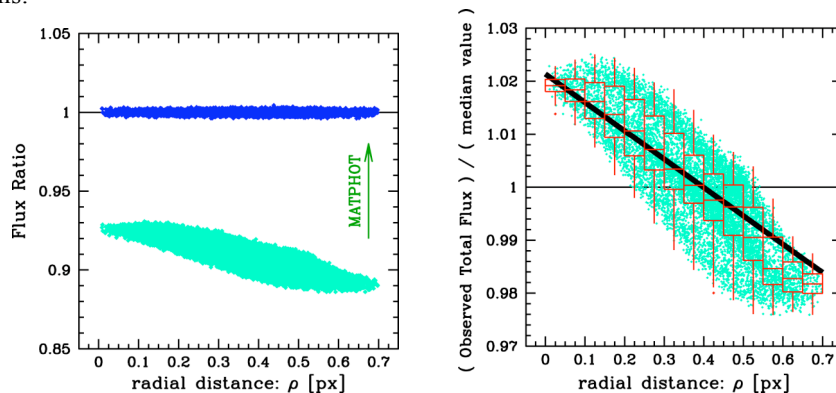


Fig. 6. Results of the MPDZ experiment with simulated IRAC Ch1

The vertical axis of the right graph of Fig. 6 shows the *observed* (apparent) total flux divided by the *median observed* total flux value of all ten thousand stars. The median values of the box-and-whisker plots (the central horizontal bar in each box) range from an excess flux of about 2% for stars centered near the center of a pixel to a flux deficit of about 2% for stars centered near the corner of a pixel. Note that this graph reproduces almost exactly the observed flux loss distribution seen in Fig. 5.1 of the IRAC Data Handbook [16]. One sees that even after the recommended flux correction (thick line of right graph of Fig. 6) is applied an approximate peak-to-peak spread of about 3% would remain for many observations – and that is exactly what is seen in Fig. 5.

6. MATPHOT PHOTOMETRY

MATPHOT PSF-fitting photometry was performed on all of the observations using MPDZ with the theoretical 5x5 supersampled IRAC Ch1 PSF shown in Fig. 1. The open diamonds in Fig. 7 show a 5.2% peak-to-peak spread in the raw measured stellar flux values reported by MPDZ.

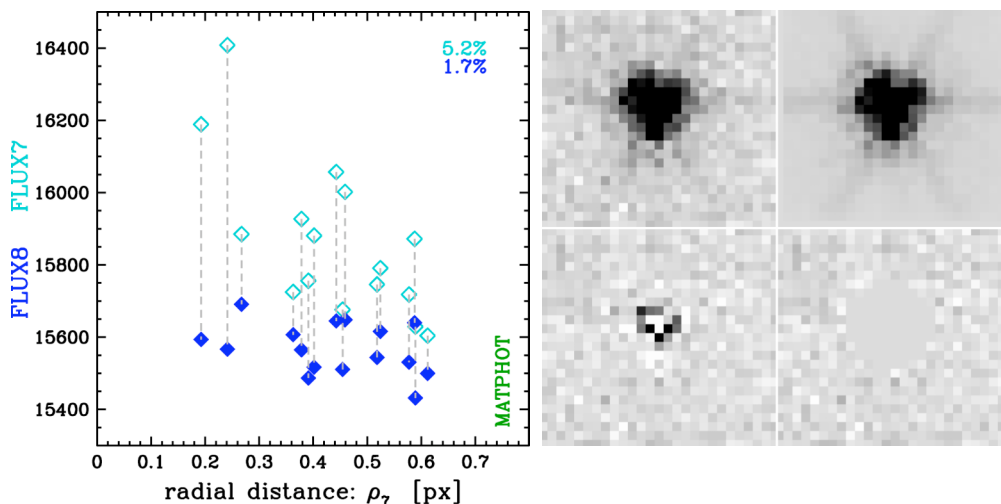


Fig. 7. MATPHOT (MPDZ) photometry

The upper-left image in Fig. 7 shows central portion of the first IRAC Ch1 observation in Table 1. The noiseless best-fit model of the observation is shown in the upper-right image. The residuals remaining after the best-fit model is subtracted from the observation are shown in the lower-left image. The lower-right image is the same as the residual image except that all residuals within a radius of 5 pixels from the fitted center of the star have been set to zero. All of these images are displayed with the same negative linear stretch which was chosen to emphasize the faint features of the stellar image.

The filled diamonds in Fig. 7 show a 1.7% peak-to-peak spread; these flux values are the combination of the raw measured stellar fluxes (open diamonds) with the sum of all of residuals (positive and negative) within a radius of 5 pixels from the fitted center of the star.

MATPHOT with residuals yield an improvement in photometric precision of more than 100% over the best results obtained with aperture photometry. The left graph of Fig. 8 compares MATPHOT photometry with residuals (FLUX8: filled diamonds in Fig. 7) with the best corrected circular photometry (FLUX6: filled circles in Fig. 5). The errorbars plotted with the FLUX8 values are the errors estimated by MPDZ for the raw MATPHOT flux estimates (FLUX7: open diamonds in Fig. 7).

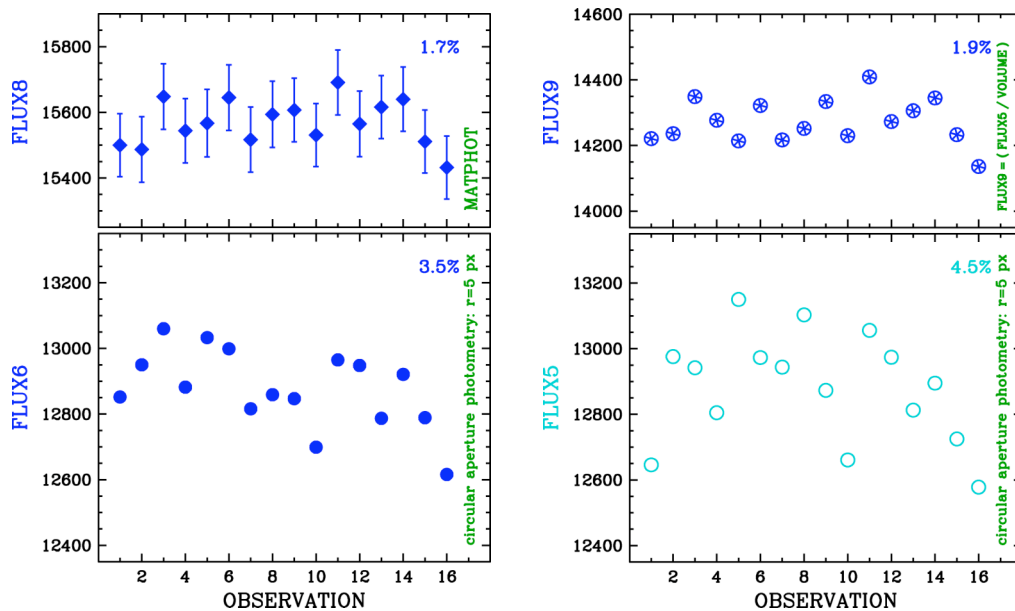


Fig. 8. Comparison between MATPHOT and aperture photometry

We see that although the recorded flux of point sources was corrupted by using lossy detectors with large intrapixel quantum efficiency variations, it is possible to significantly improve the precision of stellar photometry from observations made with such detectors – if the image formation process inside the detector is accurately modeled.

Simple aperture photometry of stellar observations obtained with IRAC Ch1 can be significantly improved by simply dividing the measured aperture flux with the volume of the Point Response Function (PRF) which is the convolution of the Point Spread Function and the discrete Detector Response Function. The right graph of Fig. 8 compares the best uncorrected circular photometry (FLUX5: open circles in Fig. 5) with those flux values divided by the volume of the best-fit PRF computed by MPDZ. The resultant peak-to-peak spread is 1.9% which is just slightly worse than the 1.7% spread from the MATPHOT with residual results. This suggests that aperture photometry from IRAC Ch1 observations could probably be significantly improved by using a two-dimensional correction function instead of using the radial correction function currently recommended in the IRAC Data Handbook. The derivation of that two-dimensional correction function would require a detailed analysis of a large number of dithered IRAC Ch1 unsaturated stellar observations.

7. SUMMARY AND DISCUSSION

This detailed analysis of multiple observations of a single bright isolated star obtained with Channel 1 of the *Spitzer Space Telescope's* Infrared Array Camera (IRAC) instrument yields an improvement in photometric precision of more than 100% over the best results obtained with aperture photometry. The improvement is achieved by accurately modeling the image formation process within lossy detectors that exhibit large intrapixel quantum efficiency variations.

Mitigating the impact of flux loss problems seen in state-of-the-art NASA-grade infrared detectors is still in its early days. Hoffmann's IRAC Ch1 intrapixel QE map [14] is the *first attempt* by the IRAC team to quantify this effect. Derivation of the intrapixel QE map is an *iterative process* due to the apparent centroid shifting caused by the non-uniform QE variation across a pixel; given an initial estimate of the intrapixel QE map, better positions of the input stellar images can then be determined, which, in turn, enables a better measurement of the intrapixel QE map to be made

Much more work remains to be done. However, the possibility of significantly improving the precision and accuracy of space-based near-infrared stellar photometry and astrometry appears to be excellent. Ground-based infrared stellar photometry can typically achieve 10% accuracy and 5% accuracy under excellent conditions; the *Spitzer Space Telescope* is currently achieving only 5% photometry despite the fact that it is a cold stable observing platform in deep space. A significant improvement to 2% photometric accuracy might now be possible with image analysis software that models the image formation process within the detector. A stretch goal of 1% photometric accuracy may even be achievable with *existing* space-based cameras using state-of-the-art near-infrared detector technology – if onboard cameras are electronically quiet and stable enough.

I wish to thank Bill Glaccum, Bill Hoffmann, David Elliott, Patrick Lowrance, and the rest of the IRAC team for their support of this research effort. This work has been supported by a grant from the National Aeronautics and Space Administration (NASA), Interagency Order No. NNG06EC81I, which was awarded by the Applied Information Systems Research (AISR) Program of NASA's Science Mission Directorate.

8. REFERENCES

1. Mighell, K. J., Stellar photometry and astrometry with discrete point spread functions, *MNRAS*, Vol. 361, 861-878, 2005
2. Kernighan, B. W. and Ritchie, D. M., *The C Programming Language* (2nd Edition), Prentice Hall, New Jersey, 1988.
3. Hanisch, R. J., et al., Definition of the Flexible Image Transport System (FITS), *A&A*, Vol. 376, 359-380, 2001.
4. Mighell, K. J., MATPHOT algorithm for digital point spread function CCD stellar photometry, *Astronomical Data Analysis II*, Proceedings of the SPIE, Vol. 4847, 207-216, 2002.
5. Mighell, K. J., The MATPHOT Algorithm for Digital Point Spread Function CCD Stellar Photometry, *Astronomical Data Analysis Software and Systems XI*, ASP Conf. Ser. 281, 387-391, 2002.
6. All source code and documentation at the MATPHOT website at NOAO:
<http://www.noao.edu/staff/mighell/matphot>
7. Levenberg, K., A Method for the Solution of Certain Problems in Least Squares, *Quarterly of Applied Mathematics*, Vol. 2, 164-168, 1944.
8. Marquardt, D., Marquardt, An Algorithm for Least-Squares Estimation of Nonlinear Parameters, *SIAM Journal of Applied Mathematics*, Vol. 11, 431-441, 1963.
9. Mighell, K. J., Accurate stellar photometry in crowded fields, *MNRAS*, Vol. 238, 807-833, 1989.
10. Mighell, K. J., Algorithms for CCD Stellar Photometry, *Astronomical Data Analysis Software and Systems VIII*, ASP Conf. Ser. 172, 317-328, 1999.
11. Fazio, G. G., The Infrared Array Camera (IRAC) for the Spitzer Space Telescope, *ApJS*, Vol. 154, 10-17, 2004.
12. Tody, D., The *IRAF* Data Reduction and Analysis System, *Instrumentation in Astronomy VI*, Proceedings of the SPIE, Vol. 627, 733, 1986.

13. Tody, D., IRAF in the Nineties, *Astronomical Data Analysis Software and Systems II*, ASP Conf. Ser. 52, 173, 1993.
14. Hoffmann, B., Intra-pixel Variation Effect on Aperture Photometry, IRAC/TMo5-028 (Simfit Report 59; Version 2: December 10, 2005), 2005.
15. Hoffmann, B., 25 Position Model Pixel Response Functions (PRF) Description and Quality, IRAC/TMo5-014 Simfit Report 52; September 3, 2005), 2005.
16. Reach, W. T., et al., Infrared Array Camera Data Handbook (Version 3.0; January 20, 2006), 2006.